**Supplemental Figures**

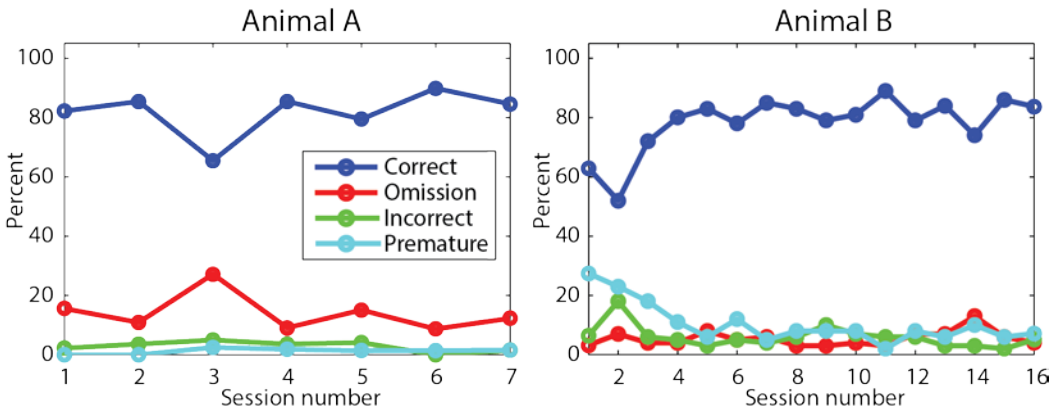


Figure S1: Behavioral performance for Animals A and B during recording sessions. Related to Figure 1.

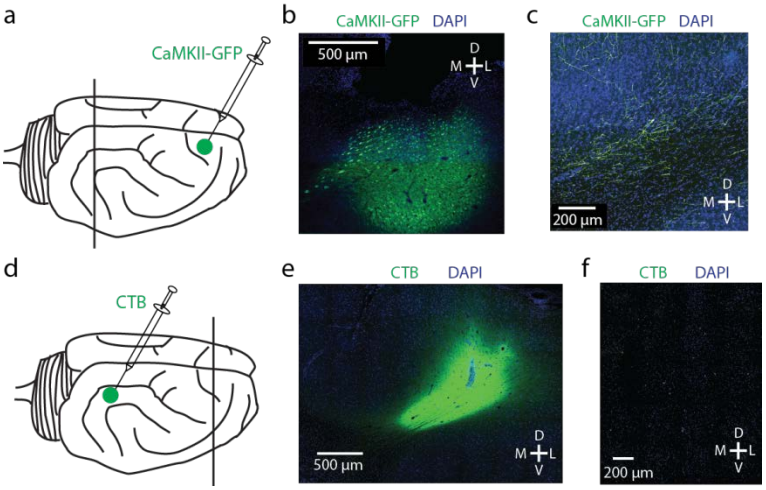


Figure S2: Anterograde and retrograde tracing demonstrate anatomical connectivity between PFC and PPC; fluorescent images in different animals from Figure 2. Related to Figure 2.

a) rAAV5-CamKII-GFP was injected in PFC for anterograde tracing.
b) Injection site in PFC shows robust labeling of cell bodies; green = GFP, blue = DAPI counterstain.
c) Projections in PPC exhibit GFP labeling, indicating direct anatomical connections from the injection site location; green = GFP, blue = DAPI counterstain.
d) CTB-488 was injected in PPC for retrograde tracing.
e) Injection site of CTB-488 in PPC at shows robust labeling; green = CTB-488, blue = DAPI counterstain.
f) PFC exhibits expression of CTB-488; green = CTB-488, blue = DAPI counterstain.

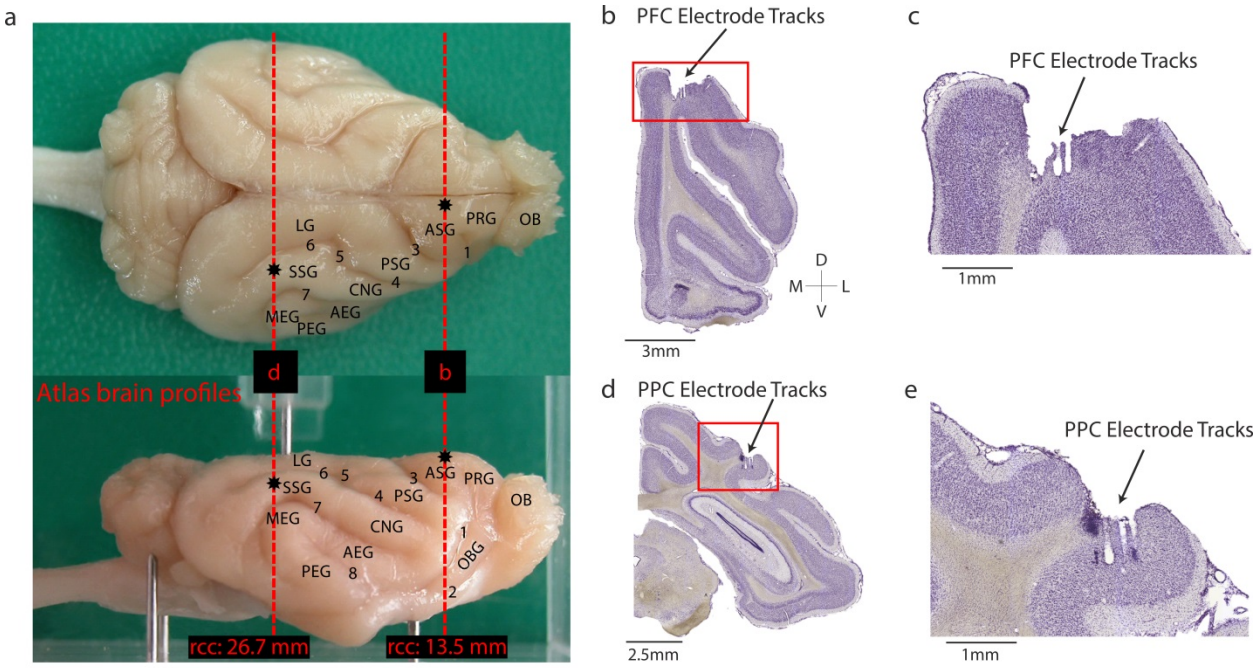


Figure S3: Recording locations in PFC and PPC. Related to Figure 2.

a) Overview of electrode implantation locations and tracer injections from ferret atlas. PFC was 27mm rcc and PPC was 13.5mm rcc. Stars indicate implantation locations. OB = olfactory bulb, OBG = orbital gyrus, ASG = anterior sigmoid gyrus, PSG = posterior sigmoid gyrus, CNG = coronal gyrus, AEG = anterior ectosylvian gyrus, MEG = medial ectosylvian gyrus, PEG = posterior ectosylvian gyrus, SSG = suprasylvian gyrus, LG = lateral gyrus, PRG = proreal gyrus; 1 = presylvian sulcus (prs), 2 = rhinal fissure (rf), 3 = cruciate sulcus (crs), 4 = coronal sulcus (cns), 5 = ansinate sulcus (as), 6 = lateral sulcus (ls), 7 = suprasylvian sulcus (sss), 8 = pseudosylvian sulcus (pss).
b) Nissl stained section in PFC show electrode implantation location in Animal A indicated by electrolytic lesions.
c) Area in red box from (b) showing electrode tracks.
d) Nissl stained section in PPC show electrode implantation location in Animal A.
e) Area in red box from (d) showing electrode tracks

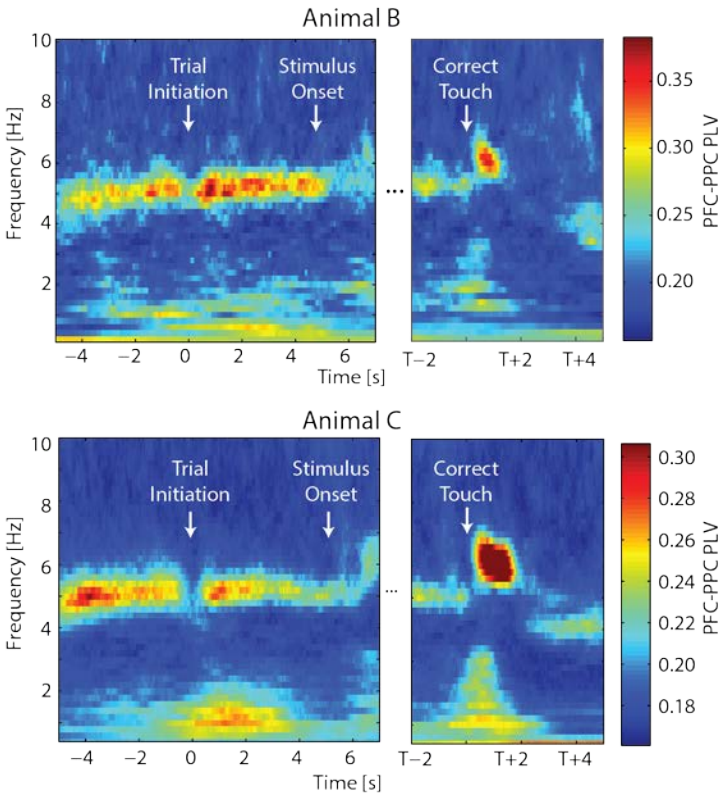


Figure S4: LFP-LFP phase locking between PFC and PPC for Animals B and C. Related to Figure 4.

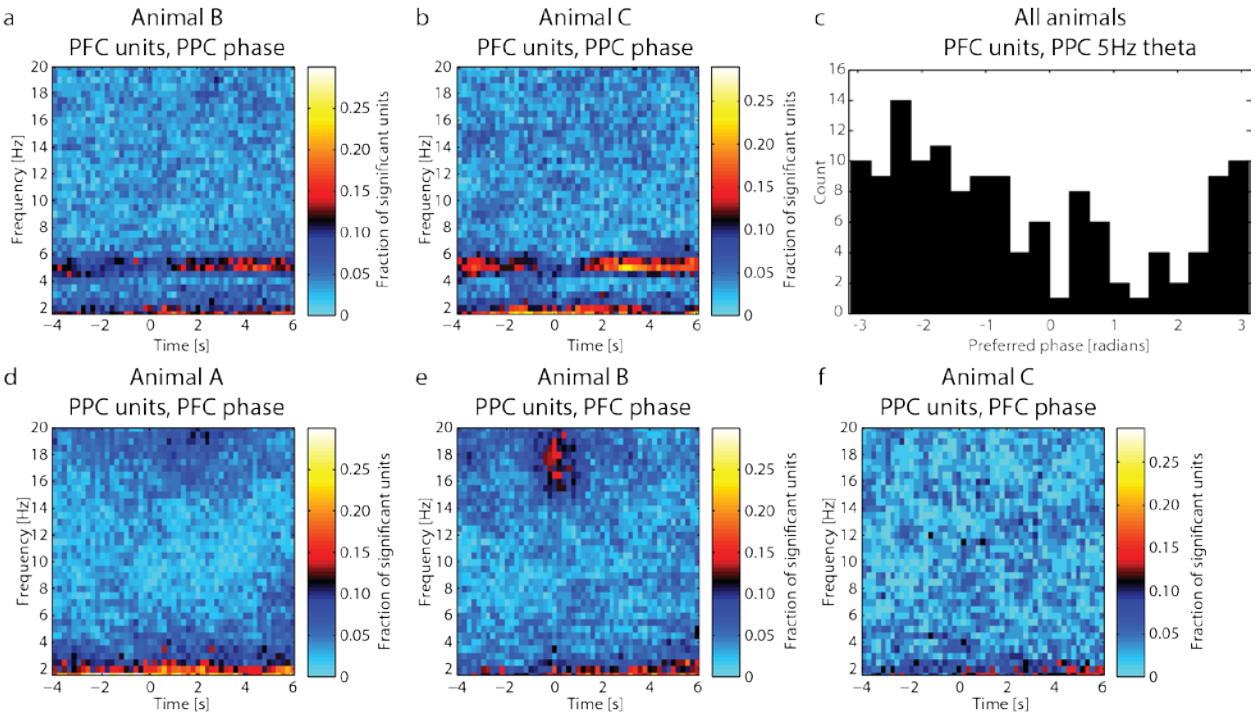


Figure S5: Fraction of units with significant spike-LFP phase locking between areas. Related to Figure 5.

a) Across recording sessions for Animal B, PFC units exhibited significant spike-LFP phase locking with PPC 5Hz oscillations.
b) Same as (a) for Animal C.
c) Distribution of preferred phases for all PFC units with significant spike-LFP phase locking to the 5Hz oscillation in PPC.
d) Across recording session for Animal A, no sizeable fraction of PPC units exhibited spike-LFP phase locking with PFC 5Hz oscillations.
e) Same as (d) for Animal B.
f) Same as (d) for Animal C.

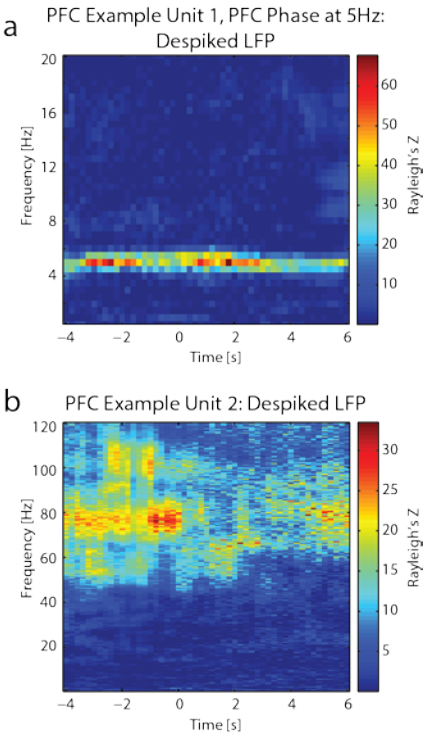


Figure S6: Spike-LFP phase locking is not an artifact of spike bleed through. Related to Figure 6.

(a) Spike-LFP phase locking of an example PFC unit calculated using despiked LFP, demonstrating coupling at 5Hz is not an artifact of spike bleed through.

(b) Same as (a) for spike-LFP phase locking in the high gamma frequency range.

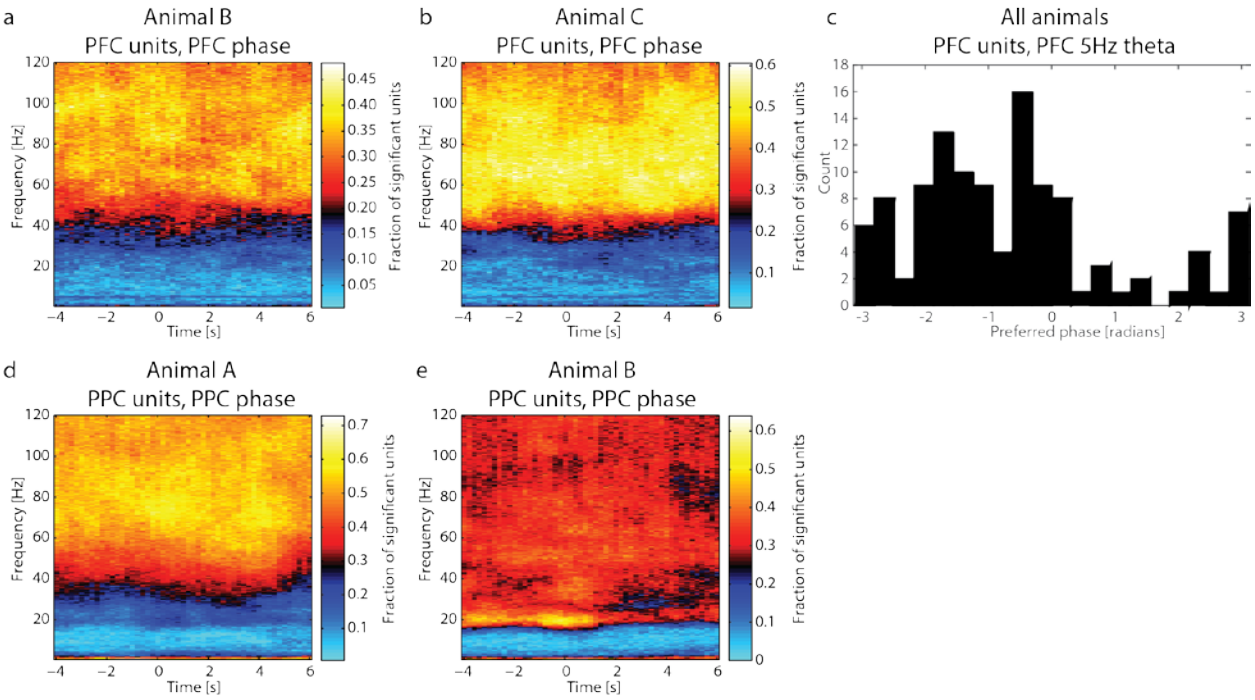


Figure S7: PFC units exhibit local spike-LFP phase locking at 5Hz and high-gamma frequencies; PPC units exhibit local spike-LFP phase locking at high-gamma frequencies. Related to Figure 6 and Figure 7.

a) Averaged across recordings for Animal B, the fraction of PFC units with significant spike-LFP phase locking across frequencies.
b) Same as (a) for Animal C.
c) Distribution of preferred phases for all PFC units with significant spike-LFP phase locking to the 5Hz oscillation in PFC.
d) Averaged across recordings for Animal A, PPC units exhibited spike-LFP phase locking at high-gamma frequencies.
e) Same as (d) for Animal B.

## Supplemental Experimental Procedures

### Behavioral Training

Spayed female ferrets (*Mustela putorius furo*, ~17 weeks old at study onset) were used in this study. Three animals were trained to perform a sustained visual attention task. Four additional animals were used for anatomical studies. All animal procedures were approved by the Institutional Animal Care and Use Committee of the University of North Carolina at Chapel Hill, and complied with guidelines set by the National Institute of Health.

We adapted the 5-choice serial reaction time task (5-CSRTT) with touch-screen implementation for this study (Bari et al., 2008). An enclosed and sound-insulated custom-built behavioral box (interior enclosure = 50 x 60 cm, exterior shell = 83 x 91 x 110 cm) was used for training and recording sessions. A capacitive touch screen (Acer T232HL bmidz 23-inch touch screen LCD display) was secured behind a plexiglass mask with 5 square openings (7 x 7 cm) to allow for response touches at one end of the enclosure, and a spout for water delivery with an infrared sensor and LED illumination was positioned near the floor on the opposing wall (Figure 1b). Auditory cues were delivered through speakers (HP Compact 2.0 speaker), a houselight was mounted on the ceiling of the enclosure, and infrared videography was performed during all sessions (Microsoft LifeCam Cinema 720p HD Webcam). The animals were trained on successive levels of increasing difficulty in order to associate the lick spout with a water reward, initiate trials at the lick spout, touch the screen, and touch the screen only in response to stimulus presentation, respectively.

Successful trial initiation was indicated by a beep (0.1 s duration) and the lick spout light turning off. Following a 5 s delay period ('sustained attention'), one of the five windows displayed a white square filling the response area for 3.5 s. A correct response was defined as touching this window during this 3.5 s stimulation period or during the 2 s following. Correct touch was indicated by immediate disappearance of the stimulus, playing of a tone (0.5 s duration), and the release of a water reward at the lick spout. Response prior to the stimulus onset (premature), touch of one of the 4 unlit squares (incorrect), and lack of any touch response (omission) were indicated by a white noise auditory stimulus (1 s duration), illumination of the house light (which was otherwise off), and a subsequent 6 s time-out period. Following the time-out period or 8 s after a correct response (sufficient time for the animal to retrieve the water reward), the lick spout light re-illuminated to indicate that the next trial could be initiated. The operation of the behavioral apparatus was controlled with custom-written MATLAB code (MathWorks, Natick, MA) and a data acquisition device (USB 6212, National Instruments, Austin, TX). Each recording session consisted of 100 trials, although some sessions were terminated early if the animal stopped initiating trials.

Animals were trained and tested once daily on a 5 days on / 2 days off schedule. During training and testing, animals were water restricted to enhance participation in the behavioral task. Training/testing was conducted in the mornings, during which time animals received water for correct responses. Supplemental water was provided in the afternoon such that each animal had access to 60mL/kg/day. Ad lib water was provided during the 2 days off. Animal weight was monitored daily to ensure sufficient hydration.

### Microelectrode Array Implantation Surgery

Upon meeting training criterion (5 consecutive days of at least 60 trials completed with less than 30% omission), animals were implanted with microelectrode arrays in both PFC and PPC. Aseptic surgical procedures were used, as previously described (Sellers et al., 2013, Sellers et al., 2015). After anesthesia induction using an intramuscular (IM) injection of ketamine/xylazine (30 mg/kg of ketamine, 1-2 mg/kg of xylazine), ferrets were intubated and deep anesthesia was maintained with isoflurane (1-2%) in 100% oxygen. Throughout surgery, end-tidal $CO_2$, electrocardiogram, partial oxygen saturation, and rectal body temperature were monitored. Body temperature was maintained between 38-39°C with a water heating blanket and end-tidal $CO_2$ was kept between 30-50 mmHg. Tissue and muscle were retraced to expose the skull surface. Two small craniotomies were made to access the right hemisphere of PFC (5 mm anterior to bregma and 2 mm lateral to the midline) and PPC (3.5 mm lateral to the midline and midway between bregma and lambda). 32-channel microelectrode arrays (tungsten electrodes oriented 4 x 8, 200µm spacing, low impedance reference electrode 1mm shorter on the same array, Innovative Neurophysiology, Durham, NC) were positioned above each craniotomy using a stereotaxic arm and slowly inserted into deep layers of cortex. Arrays were implanted using the same orientation across all animals; thus, the same brain areas were underneath the reference electrodes for all animals. Animals were allowed to recover in their home cages for at least 7 days prior to reintroduction to water restriction and recording sessions. During recovery, meloxicam was administered for pain relief (0.2 mg/kg IM injection) and clavamox was administered to prevent infection (12.5-13mg/kg, PO).

***In Vivo* Electrophysiological Recordings**

Continuous electrophysiological data were acquired at a sampling rate of 20kHz with a bandwidth of 0.1Hz to 5kHz (RHD2132 amplifier boards connected to RHD2000 USB Interface Board, Intan Technologies, Los Angeles, CA). A motorized commutator (AC32, Tucker-Davis Technologies, Alachua, FL) with custom built adapters was used to allow unencumbered animal movement during electrophysiology. Behavioral responses were recorded as digital inputs together with the electrophysiology to ensure proper synchronization of neuronal activity and behavior.

**Data Analysis**

Because the task was self-paced, we selected behavioral responses to align the trials. Specifically, trial initiation was used for alignment, and a time window ranging from 5 s before to 7 s after this time point was analyzed. The five seconds following initiation represent the sustained attention period. For a subset of analyses, we additionally looked at neuronal activity aligned to screen touch, ranging from 2 s before to 5 s after touch. We only analyzed trials with correct responses, in which the animal was facing the screen at the time of stimulus onset. To determine the position of the animal prior to stimulus onset, we manually reviewed video recordings and coded the orientation of the animal immediately prior to the stimulus onset. A small subset of trials with signal artifacts, identified as simultaneous large amplitude deflections across channels, was excluded from analysis.

The LFP was extracted by applying a phase-preserving low-pass filter (MATLAB filtfilt, 2$^{nd}$ order Butterworth filter with cutoff at 300Hz) to the raw data. Spectral analysis was performed by convolving the LFP signals with a family of Morlet wavelets (0.5 to 120Hz, step width of 0.5Hz; or 0.2 to 10Hz, step width of 0.2Hz). Standard definitions of frequency bands were used for initial exploratory analysis (delta = 0.5-4Hz, theta = 4-8Hz, alpha = 8-12Hz, beta = 12-30Hz, gamma = 30-80Hz, high gamma = 80-120Hz). We found that the LFP spectra of all animals exhibited a pronounced peak at 5Hz, and thus used this frequency for subsequent theta analysis. We also found that each animal exhibited a local peak in or close to the gamma frequency range (29Hz, 34Hz, and 33Hz, respectively) in PPC during the sustained attention period; we thus centered a 10Hz-wide band around this local peak for each animal for analysis of gamma power in PPC. To assess the difference in spectral power before trial initiation, after trial initiation, and after touch, the power within each frequency band was averaged for the 5 s prior to initiation, the 5 s after initiation (the sustained attention period), and the 5 s after touch, respectively.

Spikes were sorted into putative single units using standard methods (Offline Sorter, Plexon Inc, Dallas, TX). Spikes were detected by applying a phase-preserving high-pass filter (2$^{nd}$ order butterworth filter with cutoff at 300Hz) to raw traces and a threshold of -4*standard deviation (750 µs deadtime) to extract waveforms with 1600 µs durations. The T-distribution expectation maximization algorithm (Shoham et al., 2003) was used to sort spikes from the first 300 s of recordings in order to create unit templates. Spikes were then matched to these templates. Outlier waveforms were removed by manual inspection. Spikes with shorter than 1 ms refractory period were removed.

A structural change test (Chow, 1960, Kimchi and Laubach, 2009) was used to assess if the SU firing rate was significantly modulated over the course of the peristimulus time period (strucchange library (Zeileis et al., 2002) for R, https://www.r-project.org/). Briefly, a PSTH was calculated for each unit with bin width of 1 ms and convolved with a Gaussian window (12 ms width); a linear model was fit to the full data window, and a series of linear models were fitted to smaller data windows. An F-statistic was calculated and evaluated with a criterion of $p < 0.05$ to determine if the coefficients from the linear regressions based on the full series and the local segment were significantly different. In the case of significant differences between the full window and smaller window-based models, the point with the largest change was indicated (breakpoint).

Phase locking values (PLV) between LFP signals in the two brain regions were calculated as previously described (Lachaux et al., 1999, Liebe et al., 2012). For every possible channel pair between PFC and PPC (*m* and *n*, respectively) a value for phase locking between 0 and 1 was calculated as

$$PLV_{mn}(t, f_0) = \frac{1}{K}\left|\sum_{k=1}^{K} e^{i(\varphi_k^m(t,f_0) - \varphi_k^n(t,f_0))}\right|$$

where $K$ indicates trials, and $\varphi_k^m(t, f_0)$ and $\varphi_k^n(t, f_0)$ indicate the instantaneous phases of the two channels at frequency $f_0$ calculated using the Morlet wavelet transform. Significance was determined by the Rayleigh statistic at a significance level of $p < 0.05$ (Fisher, 1993). Summary figures show the average of significant PLV across channels pairs.

Pairwise spectral Granger causality was calculated using the GCCA Toolbox (Seth, 2010) to test for effective connectivity between PFC and PPC from 0.5 to 50Hz. The LFPs were downsampled to 200Hz after anti-alias filtering using an FIR filter. The median across channels of the LFP signals in each region was computed and

then modeled as autoregressive processes using the LWR method developed by Morf (Morf et al., 1978). Two time periods were analyzed: the 5 second delay period following trial initiation, and the 5 seconds following correct touch. We chose the model order that captured the spectral structure observed in the data for each session (ranging from 40 to 55). To estimate the statistical significance of the computed Granger causal values, we performed a permutation-based analysis followed by a false discovery rate correction.

In order to assess the degree of phase-locking of single units as a function of time and frequency, we calculated spike-LFP synchrony according to methods previously described (Totah et al., 2013). For the 12 s trials aligned by trial initiation, spike-LFP phase locking was calculated in 2 s sliding windows with 200 ms increments. Specifically, for each time window, LFP phase angles were extracted using the wavelet transform at each spike time across trials. The circular statistics toolbox for MATLAB was used for statistical analysis of spike-LFP phase synchrony (Berens, 2009). If any time window had fewer than 50 spikes, the unit was removed from analysis. Prior to calculating strength of phase locking, differences in spike rate across time for each unit were corrected for by subsampling the number of spikes in each window such that all windows had the same number of spikes. For analysis of spike-LFP phase locking within area, the phase was taken from a neighboring electrode in order to avoid potential bleed-through of spiking activity into the LFP. For analysis of spike-LFP phase locking across areas (phase from PFC, spiking in PPC, and vice versa), the LFP was averaged across channels in the phase-providing brain region and the wavelet transform was calculated on this averaged signal. The strength of spike-LFP phase locking was then calculated using Rayleigh's Z,

$$Z = nR^2$$

where $n$ spikes contribute to the mean resultant phase vector length, $R$. The p-value was computed for each time step using the approximation

$$p = e^{\left[\sqrt{(1+4n+4(n^2-R_n^2))}-(1+2n)\right]}$$

where $R_n = R \times n$ (Zar, 1999). Significant level was set at $p < 0.05$. The fraction of units exhibiting significant spike-LFP phase locking was determined by a significant estimated p-value for at least 20% of the trial.

To further ensure that potential bleed-through of spiking activity did not influence calculated spike-LFP synchrony, we created a despiked version of the LFP. Spike times were detected by applying a -4*std threshold to the high-pass filtered data (MATLAB filtfilt, 300Hz cutoff). At each spike time, 0.5 ms before the threshold crossing to 1.5 ms after the threshold crossing was cut out from the data and replaced with a linear interpolation. Calculation of within-area spike-LFP phase locking was then conducted as described above.

**Tracing Studies**

Two types of tracer studies were completed to establish the presence of direct anatomical projections from PFC to PPC. Anterograde virus, rAAV5-CamKII-GFP (titer of 6 x $10^{12}$ vg/ml; dialyzed with 350 nM NaCl and 5% D-sorbitol in PBS, UNC Vector Core, Chapel Hill, NC), was injected in PFC (n = 2 animals) and retrograde tracer Alexa 488-conjugated cholera toxin subunit B (CTB, 1% CTB in phosphate buffer, Invitrogen) was injected in PPC (n = 2 animals) (Conte et al., 2009). Similar aseptic surgical procedures were used as described above. rAAV5-CamKII-GFP or Alexa 488-conjugated cholera toxin subunit B were prepared in a 1 µL Hamilton syringe (Hamilton Company, Reno, NV). In the case of GFP injection, 1 µL of virus was delivered (0.1 µL/min) bilaterally in PFC at a depth of 0.9mm below the surface of cortex. In the case of CTB injection, 0.1 or 0.6 µL was delivered (0.1 µL/min) bilaterally in PPC at a depth of 1-1.5mm below the surface of cortex. Following injection, the needle was left in place for 10 minutes before it was slowly removed. The craniotomy was covered with bone wax, and the tissue was sutured as described above. Virus was allowed to infect for 10 weeks and CTB was allowed to express for 7-14 days.

**Histological Procedures**

Upon reaching scientific endpoint, electrolytic lesions were induced in implanted animals by passing current through the four corner electrodes of the microelectrode array (5 µA, 10 s, unipolar). Animals were humanely euthanized with an overdose of sodium pentobarbital and immediately perfused with 0.1M PBS and 4% paraformaldehyde solution in 0.1M PBS. 60 µm coronal sections of the fixed brain were prepared with a cryostat (CM3050S, Leica Microsystems). Sections from animals implanted with microarrays were separated into series and Nissl stained or stained for cytochrome oxidase (Yu et al., 2016). Sections from animals used in tracing studies were separated into series and Nissl stained, stained for cytochrome oxidase, or mounted with DAPI mounting medium (Sigma-Aldrich, St. Louis, MO). Slides were imaged using either a widefield microscope (Nikon Eclipse 80i, Nikon Instruments, Melville, NY) or a confocal microscope with 10x objective (Zeiss LSM, Zeiss, Jena, Germany).

**Supplemental References**


Bari, A., Dalley, J. W. & Robbins, T. W. 2008. The application of the 5-choice serial reaction time task for the assessment of visual attentional processes and impulse control in rats. *Nat Protoc,* 3**,** 759-67.

Berens, P. 2009. CircStat: A MATLAB Toolbox for Circular Statistics. *Journal of Statistical Software,* 31**,** 1-21.

Chow, G. 1960. Tests of equality between sets of coefficients in two linear regressions. *Econometrica,* 28**,** 591-605.

Conte, W. L., Kamishina, H. & Reep, R. L. 2009. Multiple neuroanatomical tract-tracing using fluorescent Alexa Fluor conjugates of cholera toxin subunit B in rats. *Nat Protoc,* 4**,** 1157-66.

Fisher, N. I. 1993. *Statistical analysis of circular data,* Cambridge England ; New York, NY, USA, Cambridge University Press.

Kimchi, E. Y. & Laubach, M. 2009. Dynamic encoding of action selection by the medial striatum. *J Neurosci,* 29**,** 3148-59.

Lachaux, J. P., Rodriguez, E., Martinerie, J. & Varela, F. J. 1999. Measuring phase synchrony in brain signals. *Hum Brain Mapp,* 8**,** 194-208.

Liebe, S., Hoerzer, G. M., Logothetis, N. K. & Rainer, G. 2012. Theta coupling between V4 and prefrontal cortex predicts visual short-term memory performance. *Nat Neurosci,* 15**,** 456-62, S1-2.

Morf, M., Vieira, A., Lee, D. T. L. & Kailath, T. 1978. Recursive Multichannel Maximum Entropy Spectral Estimation. *Ieee Transactions on Geoscience and Remote Sensing,* 16**,** 85-94.

Sellers, K. K., Bennett, D. V., Hutt, A. & Frohlich, F. 2013. Anesthesia differentially modulates spontaneous network dynamics by cortical area and layer. *J Neurophysiol,* 110**,** 2739-51.

Sellers, K. K., Bennett, D. V., Hutt, A., Williams, J. H. & Frohlich, F. 2015. Awake vs. anesthetized: layer-specific sensory processing in visual cortex and functional connectivity between cortical areas. *J Neurophysiol,* 113**,** 3798-815.

Seth, A. K. 2010. A MATLAB toolbox for Granger causal connectivity analysis. *J Neurosci Methods,* 186**,** 262-73.

Shoham, S., Fellows, M. R. & Normann, R. A. 2003. Robust, automatic spike sorting using mixtures of multivariate t-distributions. *J Neurosci Methods,* 127**,** 111-22.

Totah, N. K., Jackson, M. E. & Moghaddam, B. 2013. Preparatory attention relies on dynamic interactions between prelimbic cortex and anterior cingulate cortex. *Cereb Cortex,* 23**,** 729-38.

Yu, C. X., Sellers, K. K., Radtke-Schuller, S., Lu, J. H., Xing, L., Ghukasyan, V., Li, Y. H., Shih, Y. Y. I., Murrow, R. & Frohlich, F. 2016. Structural and functional connectivity between the lateral posterior-pulvinar complex and primary visual cortex in the ferret. *European Journal of Neuroscience,* 43**,** 230-244.

Zar, J. H. 1999. *Biostatistical analysis,* Upper Saddle River, N.J., Prentice Hall.

Zeileis, A., Leisch, F., Hornik, K. & Kleiber, C. 2002. strucchange: An R Package for Testing for Structural Change in Linear Regression Models. *Journal of Statistical Software,* 7.